

# Paradoxical relationship between distress and functional network topology in phantom sound perception

**Hye Bin Yoo<sup>a</sup>, Anusha Mohan<sup>b</sup>, Dirk De Ridder<sup>c</sup>, and Sven Vanneste<sup>b,d,\*</sup>**

<sup>a</sup>*Department of Neurological Surgery, University of Texas Southwestern, United States*

<sup>b</sup>*Lab for Clinical and Integrative Neuroscience, Global Brain Health Institute, Trinity College  
Institute of Neuroscience, Trinity College Dublin, Ireland*

<sup>c</sup>*Department of Surgical Sciences, Section of Neurosurgery, Dunedin School of Medicine,  
University of Otago, Dunedin, New Zealand*

<sup>d</sup>*Lab for Clinical and Integrative Neuroscience, School of Behavioral and Brain Sciences,  
University of Texas at Dallas, Richardson, TX, United States*

*\*Corresponding author: Tel.: +353-1-896-8545, e-mail address: sven.vanneste@tcd.ie*

## Abstract

Distress is a domain-general symptom that accompanies several disorders, including tinnitus. Based on previous studies, we know that distress is encoded by changes in functional connectivity between cortical and subcortical regions. However, how distress relates to large-scale brain networks is not yet clear. In the current study, we investigate the relationship between distress and the efficiency of a network by examining its topological properties using resting state fMRI collected from 90 chronic tinnitus patients. The present results indicate that distress negatively correlates with path length and positively correlates with clustering coefficient, small-worldness, and efficiency of information transfer. Specifically, path analysis showed that the relationship between distress and efficiency is significantly mediated by the resilience of the feeder connections and the centrality of the rich-club connections. In other words, the higher the network efficiency, the lower the resilience of the feeder connections and the centrality of the rich-club connections, which in turn reflects in higher distress in tinnitus patients. This indicates a reorganization of the network towards a paradoxically more efficient topology in patients with high distress, potentially explaining their increased rumination on the tinnitus percept itself.

---

## Keywords

Resting state fMRI, Functional connectivity, Centrality, Network efficiency, Rich-club, Feeder, Resilience

---

## Abbreviations

<b>AGFI</b>	adjusted goodness of fit index
<b>AIC</b>	Akaike information criterion
<b>BIC</b>	Bayesian information criterion
<b>BOLD</b>	blood oxygen-level dependent
<b>CFI</b>	comparative fit index
<b>EEG</b>	electroencephalography
<b>fMRI</b>	functional magnetic resonance imaging
<b>GFI</b>	goodness of fit index
<b>ICA</b>	independent component analysis
<b>MNI</b>	Montreal Neurological Institute
<b>RMSEA</b>	root mean square error of approximation
<b>ROI</b>	region of interest
<b>rsfMRI</b>	resting state functional magnetic resonance imaging
<b>TE</b>	echo time
<b>TQ</b>	Tinnitus Questionnaire
<b>TR</b>	repetition time
<b>TRI</b>	Tinnitus Research Initiative
<b>VAS</b>	visual analog scale

---

## 1 Introduction

Functional brain connectivity is a framework of complex information processing (Friston, 2010) where brain regions (nodes) are organized in a cost-effective manner called the “small-world” topology (Bullmore and Sporns, 2012; Watts and Strogatz, 1998). The different properties of functional brain networks are affected in several pathologies (Stam, 2014), including tinnitus (Mohan et al., 2016a,b, 2017). Tinnitus is the perception of a phantom sound in the absence of a physical sound source (Eggermont and Roberts, 2004). About 10% of the population experience tinnitus (Eggermont and Roberts, 2004) and up to 25% of patients report a significant, negative impact on their quality of life (Heller, 2003). Tinnitus is accompanied by a non-zero loudness component and a variable emotional/distress component (De Ridder et al., 2014). Although the loudness is unique to auditory phantom percepts, distress is a domain-general construct that presents in other disorders such as chronic pain, post-traumatic stress disorder, dyspnea in asthma, social rejection, and functional somatic syndromes such as electro-sensitivity to mobile phones (Kross et al., 2007; Landgrebe et al., 2008; Moisset and Bouhassira, 2007; von Leupoldt et al., 2009; Wager et al., 2013).

Tinnitus distress exhibits a physiological similarity with these different disorders manifesting as pathological changes in functional connectivity among cortical and subcortical regions in resting state networks (Chen et al., 2017; De Ridder et al., 2011; Imperatori et al., 2014; Song et al., 2015; Vanneste et al., 2014). Although the neural correlates of tinnitus distress has been explored in the past, its relationship with different network properties needs further investigation. One would hypothesize that brain networks of highly distressed individuals might exhibit lower efficiency of information transfer between brain regions. However, in our most recent study using resting state EEG, we showed that the network of tinnitus patients with high distress showed a paradoxical balance between local and long distance connectivity, suggesting optimal efficiency of information transfer (Mohan et al., 2018). On similar lines, studies from other pathologies also show that patients suffering from late-life depression and post-traumatic stress disorder exhibit higher brain network efficiency compared to healthy individuals (Lei et al., 2015; Lo et al., 2015; Zhang et al., 2011). Although our previous study suggested the possible relationship between distress and efficiency (Mohan et al., 2018), we did not delve into this relationship empirically. Thus, in the current study we specifically aim to investigate the relationship between tinnitus distress and efficiency of information transfer between brain regions and how it is influenced by different network properties using resting state functional magnetic resonance imaging (rsfMRI).

The small-world topology is orchestrated by a core-periphery structure in which the functional core substrate consists of densely connected regions with overlapping peripheral modules that are integrated to the core (Holme, 2005; Yang and Leskovec, 2014). The densely connected core is called the “rich club” and the peripheral modules consist of “feeder” and “local” regions (McAuley et al., 2007; Senden et al., 2014; van den Heuvel and Sporns, 2011). The feeder regions connect directly to the rich-club regions; whereas the local regions connect with one another (van den Heuvel and Sporns, 2011). This way the small-world topology maintains a subtle balance between the two opposing functions—functional integration (long-distance connectivity) and segregation (local connectivity) (McAuley et al., 2007; Senden et al., 2014; van den Heuvel and Sporns, 2011). Functional integration is directly proportional to the efficiency of the network whereas segregation is inversely proportional (Rubinov and Sporns, 2010).

In addition, the small-world topology also exhibits a balance between resilience to external attacks and the efficiency of communication between brain regions (Peng et al., 2016). Resilience is the capacity of a network to absorb change while retaining much of its original properties (Holling, 1973). A previous study that mimicked physiological disturbances such as trauma and degeneration to brain networks through a virtual lesion to rich-club hubs and feeder regions showed that network properties were better preserved (more resilient) when rich-club hubs were removed rather than feeder (Mohan et al., 2017). This was because feeder regions presented with higher betweenness centrality, i.e. these were regions through which many of the shortest paths between two arbitrary nodes passed, explaining the increased vulnerability of these regions to attacks compared to rich club regions (Mohan et al., 2017). Previous studies have also described a trade-off between resilience

and network efficiency. These studies showed that trying to increase the efficiency of communication leads to reorganization of the network with low resilience to attacks and vice-versa (Brede and de Vries, 2009; Netotea and Pongor, 2006; Peng et al., 2016).

From the above studies, we gather that network efficiency is directly or indirectly related to several network properties such as functional integration, segregation, small-worldness index, betweenness centrality of rich-club and feeder regions and resilience index of removing rich-club and feeder connections. Therefore, in the current study we will analyze the direct and indirect relationship between tinnitus distress and network efficiency by determining the correlation between tinnitus distress and the above-mentioned network measures. Furthermore, we will perform a path analysis to determine how these different variables predict the relationship between tinnitus distress and network efficiency. We propose a positive relationship between the efficiency of the tinnitus network and tinnitus-related distress mediated by the resilience and centrality of the rich-club and feeder connections. This would also suggest an association between the reorganization of network topology and tinnitus distress. Since distress is a domain-general construct, the relationship established in the current study could serve as a hypothesis for other disorders as well.

---

## 2 Materials and methods

This study calculated the functional connectivity between brain regions by correlating the corresponding time series of resting state BOLD signals from different brain regions. Subsequently, functional connectivity matrices between 105 regions of interest were constructed for each participant. Graph theoretical analysis was employed on each individual's connectivity matrix to analyze the topological parameters and resilience against the removal of rich-club and feeder connections. A detailed explanation of these methods is given in the following subsections.

### 2.1 Study participants

This is a cross-sectional study that recruited ninety chronic tinnitus outpatients from the multidisciplinary Tinnitus Research Initiative (TRI) Clinic of the University Hospital of Antwerp, Belgium. Subjects with pulsatile (objective) tinnitus, Ménière's disease, otosclerosis, chronic headaches such as pathological migraines, neurological disorders such as brain tumors, and individuals who were being treated for mental disorders were excluded. All subjects provided written informed consent, complying with the Declaration of Helsinki 2000. This study was approved by the local ethical committee of the Antwerp University Hospital. The demographics and clinical/audiological features of the tinnitus group are shown in Table 1. We do not use a control group in this study since we are more interested in the correlation between network properties and

**Table 1** Demographic information.

Variable (total $n = 90$ )	Min	Max	Mean $\pm$ SD
Age	18	81	47.81 $\pm$ 13.75
Onset age	15	77	42.66 $\pm$ 14.00
TQ score	2	72	35.02 $\pm$ 17.02
LOUD (0–10)	1	10	5.37 $\pm$ 2.30
HL (dB hearing level)	2.78	76.67	25.67 $\pm$ 16.06
DUR (years)	0.13	25	5.22 $\pm$ 5.29

Abbreviations: SD, standard deviation; TQ, Tinnitus Questionnaire; LOUD, subjective level of loudness represented by visual analogue scale; HL, averaged hearing loss; DUR, duration of the disease.

tinnitus distress. Specifically, we propose a model that can explain the influence of different network properties on the relationship between distress and efficiency of network reorganization.

## 2.2 Audiological and behavioral assessments

Pure tone audiometric thresholds characterizing the extent of hearing loss (in decibels hearing level, dB HL) were measured at 0.125, 0.25, 0.5, 1, 2, 3, 4, 6, and 8 kHz in accordance with the British Society of Audiology (Audiology, 2008). The level of hearing loss at each frequency was calculated as the numerical average of the hearing thresholds across both ears.

The pitch and loudness of the tinnitus percept was recorded by matching the emulated tinnitus tone for each patient. For subjects with unilateral tinnitus, the ear with no tinnitus was tested. For subjects with bilateral tinnitus, the ear contralateral to the worse tinnitus was tested. The patients with pure tone tinnitus were initially presented with a 1-kHz pure tone and patients with narrow-band noise were presented with 1/3 octave-band noise centered at 1 kHz. These stimuli were presented at 10 dB above their hearing threshold at that frequency. The frequency of the stimulus was adjusted until the patient verified that the presented sound most closely matched the pitch of the perceived tinnitus. The loudness of the perceived tinnitus was matched to the loudness of the stimulus in the same way. The tinnitus loudness (in decibels sensation level, dB SL) was computed as the difference between the absolute tinnitus loudness and the hearing threshold in dB HL at that frequency (Meeus et al., 2009, 2011).

The subjective level of loudness in tinnitus was assessed using a Visual Analogue Scale (“how loud is your tinnitus?”) on a 10 cm horizontal line going from minimum to maximum). The distress associated with tinnitus was measured using the Dutch translation of the Tinnitus Questionnaire (TQ) validated by Meeus and colleagues (Hallam, 1996; Meeus et al., 2007). A broad spectrum of tinnitus-related psychological complaints were measured using 52 items on the TQ, which included emotional and cognitive distress, intrusiveness, auditory perceptual difficulties,

sleep disturbances, and somatic complaints (Hiller and Goebel, 1992; McCombe et al., 2001) caused by tinnitus. Each item was scored on a three-point scale, ranging from “true” (2 points), to “partly true” (1 point), to “not true” (0 points), with a score range of 0–84 points in accordance with previous studies (Hiller and Goebel, 1992; Hiller et al., 1994; Meeus et al., 2007). The total TQ score was considered the measure for tinnitus distress. Finally, a bivariate Pearson correlation was performed between the different behavioral variables such as age, duration, hearing loss, VAS for loudness and TQ score for distress.

## 2.3 Magnetic resonance imaging

### 2.3.1 Acquisition

Structural T1 images were acquired using the MPRAGE protocol of the 3.0 Tesla Siemens Trio scanner. The protocol used a repetition time (TR) of 2300 ms, an echo time (TE) of 2.94 ms, an inversion time of 900 ms, and a flip angle of  $9^\circ$ . 160 sagittal slices were recorded using a matrix size of  $256 \times 256$ , at a  $1 \times 1 \times 1 \text{ mm}^3$  resolution.

The resting state functional magnetic resonance images (rsfMRI) were obtained using echo-planar imaging protocol with online motion correction of the same scanner. TR was set at 3000 ms, TE at 30 ms, and flip angle of  $90^\circ$  to acquire 50 axial slices in descending order for 140 time points at  $2.5 \times 2.5 \times 2.8 \text{ mm}^3$  spatial resolution.

### 2.3.2 Preprocessing

MR images were preprocessed using Statistical Parametric Mapping (SPM12b, Wellcome Department of Imaging Neuroscience, University College London, UK). High-resolution structural images were normalized to the standard Montreal Neurological Institute (MNI) template and segmented for three structural components: gray matter, white matter, and cerebrospinal fluid. Functional images were realigned in six degrees of freedom to correct for motion artifacts, and then after co-registration of functional volumes to the structural image (T1), volumes that contained extreme movements were linearly regressed out as covariates using the Artifact Detection Tool (Gabrieli Lab, MIT, US, [http://www.nitrc.org/projects/artifact\\_detect/](http://www.nitrc.org/projects/artifact_detect/)). Co-registered functional images were normalized to the standard MNI template using nonlinear transformation parameters acquired by the process of normalizing structural images to the standard space (Ashburner and Friston, 1999; Friston et al., 1995).

The images were further processed to account for motion-related and physiological noises using independent component analysis (ICA) in CONN functional connectivity toolbox (Whitfield-Gabrieli and Nieto-Castanon, 2012). Confounding factors of signals from white matter and cerebrospinal fluid were linearly regressed out from the global signal using aCompCor (Behzadi et al., 2007). The data were parcellated using Harvard-Oxford cortical and subcortical structural atlases (Desikan et al., 2006; Frazier et al., 2005; Makris et al., 2006). Regions of interest (ROIs) included 105 cortical and subcortical structures defined by the atlas, not

including the brainstem and cerebellum. The list of regions used is provided in Supplementary Table 5 (Supplementary material in the online version at <https://doi.org/10.1016/bs.pbr.2020.08.007>). The time series of the BOLD signal was calculated in each ROI by taking the average value across all voxels included in that ROI.

## 2.4 Wavelet transformation and construction of frequency-specific connectivity matrix

Wavelet transform decomposes different frequency bands to analyze details of signals at each band (Percival and Walden, 2000). Discrete wavelet transform is a linear operation that discretely samples the details out of the original signal. In this study, wavelet transform was performed using the packaged “wavelets” in R (R Core Team, Vienna, Austria. <http://www.R-project.org>) (Aldrich, 2010; Percival and Walden, 2000; Team, 2013). Maximum overlapped discrete wavelets transform was used with Haar wavelets to decompose the BOLD signals into 0.083–0.167 Hz, 0.042–0.083 Hz, 0.021–0.042 Hz, and 0.010–0.021 Hz bands, given that the sampling rate in fMRI acquisition protocol is 0.333 Hz (TR = 3 s) (Hsu et al., 2005).

Based on previous literature, we focused on the signals in 0.042–0.083 Hz frequency band. The 0.040–0.070 Hz band specifically appears to be less affected by physiological artifacts (Glerean et al., 2012), i.e. vascular signals (D’Esposito et al., 2003), and more is functionally relevant compared to the slower or faster bands (Biswal et al., 1995; Ponce-Alvarez et al., 2015). This study extracted the closest frequency band that is 0.042–0.083 Hz, which is given by the analytic outcome of wavelet transform with the Nyquist frequency of 0.167 Hz. We calculated functional connectivity using the bivariate wavelet correlation between wavelet coefficients from two different brain regions, using WMTSA toolbox version 0.2.6 for MATLAB (The MathWorks, Inc., Natick, Massachusetts, United States) (Percival and Walden, 2000). For further graphical analyses of connectivity matrices, negative connectivity values were regarded as zero.

## 2.5 Construction of real and random networks

Graph theory was employed to examine the topological characteristics of each network, where brain regions corresponded to nodes and functional connections to edges. Graph theory provides a mathematical framework to model and quantify pairwise relationships between objects in a variety of fields such as computer science, physics, chemistry, social science, biology etc. It defines a set of network-based properties such as degree of functional integration and segregation, efficiency of information transfer, resilience to damage etc. which provides a holistic description of the topological organization that results from the pairwise relationships between the different objects. In doing so, graph theory offers a well-rounded method to study the communication between different sets of objects in the network. The Brain Connectivity Toolbox for MATLAB™ was used to analyze graph-theoretical metrics

(Rubinov and Sporns, 2010). Functional connectivity matrices formed by the bivariate wavelet correlations between coefficients constituted the real networks. The real functional connectivity matrices were weighted between 0 and 1. One hundred undirected (symmetrical), random functional connectivity matrices were created for comparison. The weights of the edges in each random matrix were assigned via random permutations of sampled values from a Gaussian distribution ranging from 0 to 1, whose mean and standard deviation was equal to that calculated across the individual networks. For further analyses, negative correlations were counted as zeros.

## 2.6 Proportional thresholding of real networks

The proportional cost of functional connectivity is computed as the ratio of the number of edges to the total possible number of edges within the network (Latora and Marchiori, 2003). Differences in the cost across individuals are known to have major effect on the quantification of network measures (van den Heuvel et al., 2017). Furthermore, the number of edges can bias the results, by either excluding the false negative connections or including the false positive connections (Zalesky et al., 2016). Accordingly, the cost has to be controlled to have consistent values across subjects within a group, and multiple network costs should be used for analyses to verify if the computation results are affected by the absolute value of the cost (Achard and Bullmore, 2007; Zalesky et al., 2016).

In this study, a Minimal-spanning-tree based algorithm is adopted (Hagmann et al., 2008; Hidalgo et al., 2007; Rubinov and Sporns, 2010) to keep the proportional costs across individuals the same. This algorithm connects all the nodes together within a network while selecting the edges with the highest weights and avoiding the loops as much as possible. By applying it on each individual, the proportional costs of the networks can be thresholded to have designated values. Here, individual networks have been thresholded multiple times to have costs ranging from most scarce 10% to most dense 55%, incrementing by 5%. The maximum cost of 55% was determined because the individual with the lowest level of raw connectivity cost had the value of 59.5%, which is  $< 60\%$ . Network measures were evaluated for each individual, and the evaluation was repeated for all the cost values from 10% to 55%. For each calculation, the random matrices were constructed to have the same number of edges as the real matrices.

## 2.7 Network measures

### 2.7.1 Global efficiency

The global efficiency of a network is a measure of the speed of information transfer (Latora and Marchiori, 2001), in this case between two brain regions. This metric represents the sum of the reciprocals of the number of edges a node requires to connect itself to the other nodes within the network (Rubinov and Sporns, 2010). In graph theory, the functional distance between two regions is inversely proportional to the connectivity strength between the two regions. If the functional distance

between two regions is lower, the global efficiency of information transfer between the two regions is higher (Rubinov and Sporns, 2010). Thus, global efficiency is inversely proportional to the functional distance across brain regions, which is represented as characteristic path length defined in the following section.

### **2.7.2 Characteristic path length**

The characteristic path length is an empirical measure of network integration that accounts for the shortest functional distance (Boccaletti et al., 2006) connecting any two regions in the brain. The functional distance is calculated as the inverse of the functional connectivity matrix. The shortest distance between pairwise brain regions was calculated using Dijkstra's algorithm that yields the functional distance matrix (Rubinov and Sporns, 2010).

### **2.7.3 Clustering coefficient**

The clustering coefficient represents the level of network segregation by identifying the neighbors of each node and determining the degree of local connectivity of that node with its neighbors (Schank and Wagner, 2004). It is estimated by calculating the number of triangles around a node and averaging this quantity across all nodes in the network (Rubinov and Sporns, 2010). The clustering coefficient of each region was averaged to represent every individual network's degree of segregation.

### **2.7.4 Small-worldness**

A network's small-worldness index is calculated as the fraction of the relative clustering coefficient over the relative characteristic path length of the network (Watts and Strogatz, 1998). The relative network measures are calculated as the ratio of an individual's characteristic path length and clustering coefficient to that of the average values from 100 random networks. The formula for calculating small-worldness is given in Watts and Strogatz (1998) and Humphries and Gurney (2008).

### **2.7.5 Edge-betweenness centrality of rich-club and feeder edges**

Edge-betweenness centrality quantifies the importance of a connection, which is defined as the number of shortest paths between pairs of nodes that are connected via the current edge (Cuzzocrea et al., 2012; Girvan and Newman, 2002). Edges with higher betweenness centrality are more important for connecting distinct clusters within the network. Removing many of these edges will disintegrate the network structure. In this study, the average edge-betweenness centrality of rich-club and feeder edges was calculated to identify their importance in individual network structures and also to correlate with distress.

### **2.7.6 Network resilience against rich-club and feeder connections**

Network resilience represents how much of network efficiency an individual's functional network loses as a result of damaging a fixed number of connections (Alstott et al., 2009). It has been previously defined as the rate of change in global efficiency, which is the global efficiency of the damaged network over that of the original

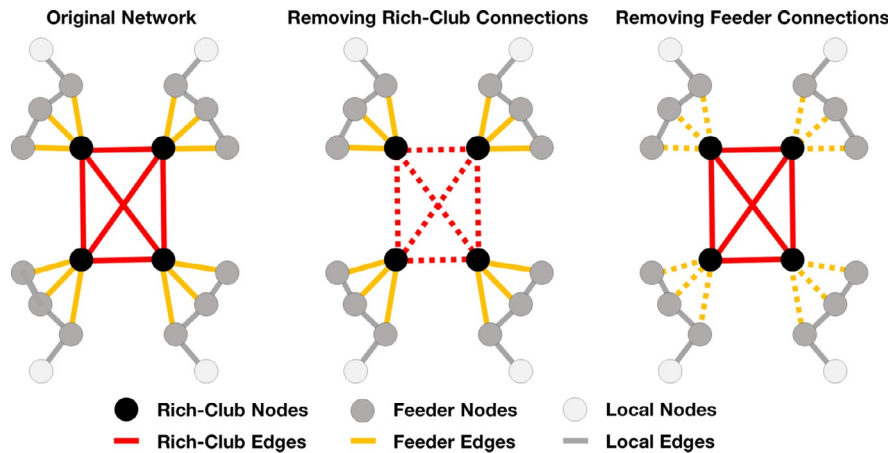
network (Netotea and Pongor, 2006). This study simulated the damages by introducing zero for the connectivity weight of a targeted edge and its transposed location within the network. Network resilience was computed based on damage to both rich-club and feeder connections. The classification of rich-club and feeder connections was done as follows.

The rich-club nodes are densely connected nodes that play an important role linking distant brain regions across the network (van den Heuvel and Sporns, 2011). The rich-club nodes were defined using the procedures established in previous studies (Colizza et al., 2006; van den Heuvel and Sporns, 2011). The normalized rich-club coefficients of a real network is defined as rich-club coefficients of a real network divided by the average values of the random networks (van den Heuvel and Sporns, 2011). In this study, normalized coefficients were calculated for each real network using the averaged rich-club coefficients of the 100 random networks. To verify if the rich-clubs in real networks had significantly higher rich-club coefficients than those of the random ones, the 90 normalized rich-club coefficients were compared if they were larger than the value one using one-sample *t*-test (Bonferroni-corrected  $P < 0.05/105$ ) (Collin et al., 2014). We selected the ROIs with normalized rich-club coefficients verified to be greater than one and regarded the ROIs with the highest degree values in each individual network as rich-clubs. As a rule of thumb, the largest possible number of the nodes considered to be rich-clubs was set at 12% of a total of 105 nodes, i.e. 13 nodes (Collin et al., 2014). The connections between any pairs of rich-clubs were defined as the rich-club edges, and the ones between the rich-clubs and nodes that directly connect to the rich-clubs were defined as feeder edges.

The important edges (rich-club and feeder) and their removal process are visualized in Fig. 1. The simulation of damaging edges was performed by removing the rich-club or feeder edges one by one from individual networks in a shuffled order. The global efficiency values were calculated per the removal of each edge, and then the rate of change of global efficiency over the number of edges removed served as the measure of network resilience. In other words, the linear regression coefficient predicting the global efficiency by the number of edges removed indicated the degree of resilience. Linear regression was evaluated using the MATLAB Statistics Toolbox with the number of edges removed as the independent variable and global efficiency as the dependent variable. The slope or regression coefficients are always negative, and higher values indicate greater resilience. The network resilience was calculated for 20 random trials of edge removal, and the regression coefficients were averaged across trials to obtain resilience to damage of rich-club or feeder edges. The most common and least common rich club nodes were also identified and this process is explained in detail in the Supplementary material in the online version at <https://doi.org/10.1016/bs.pbr.2020.08.007>.

## 2.8 Statistical analysis

The level of distress (TQ score) was correlated with the aforementioned network properties—global efficiency, characteristic path length, clustering coefficient, small-worldness, average edge-betweenness centrality and network resilience—of

**FIG. 1**

Representation of functional connectivity and rich-club or feeder regions. Targeted removal of rich-club and feeder edges are visualized as dotted lines.

the rich-club and feeder connections. Partial correlation with distress was performed by controlling for age, mean hearing loss, tinnitus loudness (VAS score), and the duration of the tinnitus (significant at two-tailed  $P < 0.05$ ). Further, distress was correlated to the centrality and resilience measures for rich-club and feeder edges using partial correlation. The interdependence between network measures has been evaluated using Pearson's bivariate correlation (significant at two-tailed  $P < 0.05$ ). Firstly, relation between efficiency and centrality of rich-club or feeder edges was identified. Secondly, trade-off of efficiency and resilience against removing rich-club and feeder edges was computed. All the correlation analyses were performed per every proportional cost ranging from 10% to 55%.

## 2.9 Path analysis

This study applied path analysis between the network measures and distress to identify their relationship. According to our hypothesis, the relationship between distress and efficiency of information transfer between regions is significantly mediated by other network properties. To build the model described, we verified that there exists significant correlation of distress, as well as significant interdependence of efficiency to all the network measures within a model. In previous analyses, centrality of feeder edges and resilience against removing rich-club edges were found to be irrelevant to efficiency or distress, thus they were not included in the model. Given the network costs of 45% and 50%, the correlations of distress and efficiency were verified with centrality of rich-club edges and resilience against removing feeder edges. Thus, the causal model was built at the costs of 45% and 50% using the aforementioned network measures and distress.

SPSS AMOS (Arbuckle, 2013) was used to test the goodness-of-fit of path models and estimate the parameters using maximum likelihood estimation. Three models (denoted A, B, C) that have three sub-models each were tested. Model A represents the associations where the network efficiency indirectly predicts distress. Model B represents the associations where distress indirectly predicts the network efficiency. Model C represents the loop association where each variable predicts at least one other in the model, and none of the variables is solely independent. The sub-models for A, B and C were defined as: (Xia et al., 2013) no direct contribution between network efficiency and distress once resilience against feeders' removal and rich-clubs' centrality were considered; (van den Heuvel et al., 2012) network efficiency directly predicts distress in addition to feeders' resilience and rich-clubs' centrality; and (Honey et al., 2010) distress directly predicts network efficiency in addition to feeders' resilience and rich-clubs' centrality. In total, nine models will be tested and compared. In all tested models, the causal relationship between distress and network measures should also represent the partial correlation controlled for age, mean hearing loss, loudness and duration. Thus, all the variables included in the model were put as standardized residuals of each variable regressed by the behavioral covariates other than distress.

## 2.10 Comparison of models

Indices for absolutely determining whether the model describes the relationship well enough were given using goodness-of-fit (GFI), adjusted GFI (AGFI) and root mean square error of approximation (RMSEA). GFI higher than 0.95, AGFI and RMSEA under 0.06 are considered to be acceptable for a model (Schreiber et al., 2006). For relatively determining which model describes the relationship the best among the hypothesized, we used comparative fit index (CFI), Akaike information criterion (AIC), and Bayesian information criterion (BIC) and then compared these measures between models to find the highest CFI, lowest AIC, and lowest BIC (Schumacker and Lomax, 2012). Parameter estimates for the linear regression between variables are shown for the best model only.

---

## 3 Results

### 3.1 Behavioral factors

There exists a strong positive correlation between hearing loss and age, TQ score, loudness and duration; loudness and TQ score and duration. The relationship among all tinnitus-related behavioral measures is presented in Table 2.

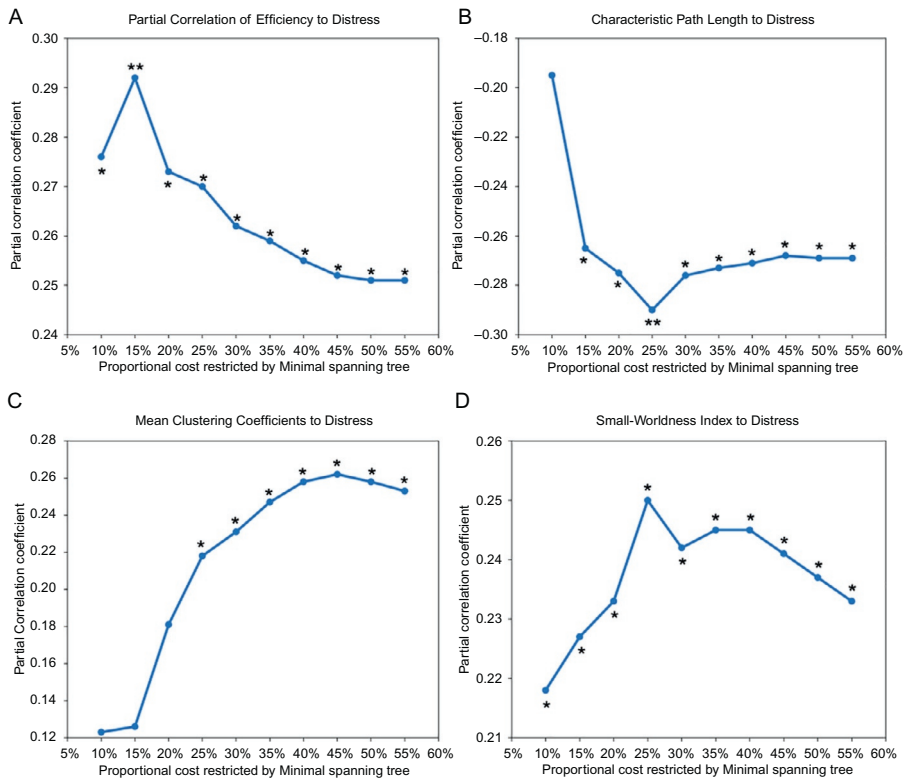
### 3.2 Distress severity and network measures

Different topological measures were correlated with tinnitus distress using partial correlation (Fig. 2), controlling for the other behavioral covariates. As a result, distress levels were significantly correlated to the individual network efficiency in a

**Table 2** Correlation of behavioral measures in tinnitus.

	Age	TQ	LOUD	HL	DUR
Age		$r=0.08$	$r=0.18$	$r=0.55$ **	$r=0.15$
TQ			$r=0.41$ **	$r=0.38$ **	$r=0.14$
LOUD				$r=0.37$ **	$r=0.33$ **
HL					$r=0.28$ **
DUR					

Abbreviations: TQ, Tinnitus Questionnaire; LOUD, Subjective level of loudness represented by visual analogue scale; HL, Averaged hearing loss; DUR, Duration of the disease. Significant correlations are marked with stars (two-tailed \*\*  $P < 0.01$ ).

**FIG. 2**

Partial correlation of tinnitus-related distress to network measures is represented across different levels of proportional network costs; (A) global efficiency, (B) characteristic path length, (C) mean of clustering coefficient, and (D) small-worldness index. All analyses are controlled for age, mean hearing loss, loudness and durations. X-axis represents the proportional costs ranging from 10% to 55%, restricted using Minimal spanning tree algorithm. Y-axis is the partial correlation coefficient of distress to each measure (\* two-tailed  $P < 0.05$ , \*\*  $P < 0.01$ ).

positive direction for all tested proportional costs (10–55%). The characteristic path length of individual networks was inversely correlated with distress showing negative correlation, but the tendency was not significant for 10% cost. The mean clustering coefficients showed positive correlation to distress, but only when the cost was higher than 20%. Finally, the small-worldness index was found to be correlated in positive direction with distress for all costs. In addition, a bivariate correlation analysis showed that efficiency significantly increases as small-worldness increases for all network costs (minimum  $r=0.727$  at 10% cost,  $P<0.001$ ). Together, the results show that more distressed individuals have more topologically efficient network organization.

### **3.3 Distress severity and edge-betweenness centrality of selected edges**

Partial correlation analysis of the edge-betweenness centrality of rich-club and feeder edges and distress is summarized in Fig. 3. The present results showed that the higher the distress, the lower the centrality of rich-club edges in one's network, but only when the costs were as high as 30% and 40% or higher. The effect was not statistically significant for the centrality of feeder edges for any costs.

### **3.4 Distress severity and network resilience against removing selected edges**

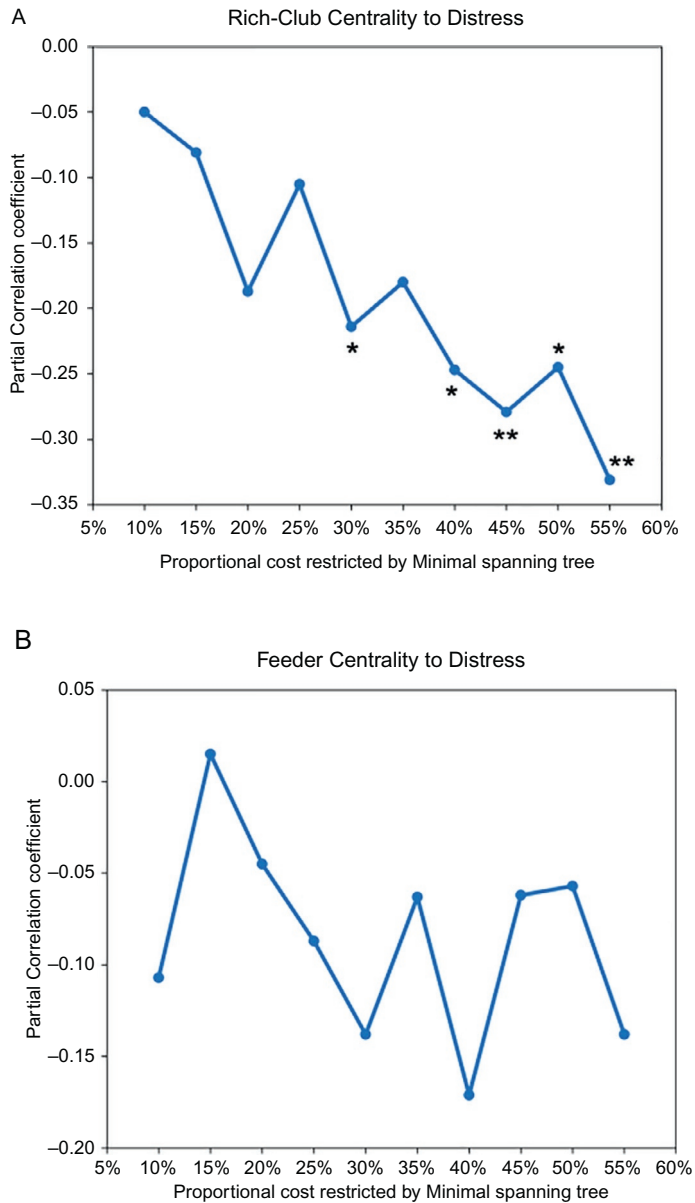
Partial correlation between network resilience and distress is demonstrated in Fig. 4. The level of resilience is always negative, since it represents the decrease in the rate of global efficiency as edges are removed. Tinnitus distress was positively correlated with the resilience of rich-club edge removal when the network was most dense i.e. at costs 50% and 55%. On the other hand, tinnitus distress was negatively correlated with the resilience of feeder edge-removal at higher costs i.e. 45% and 50%.

### **3.5 Network efficiency and centrality of selected edges**

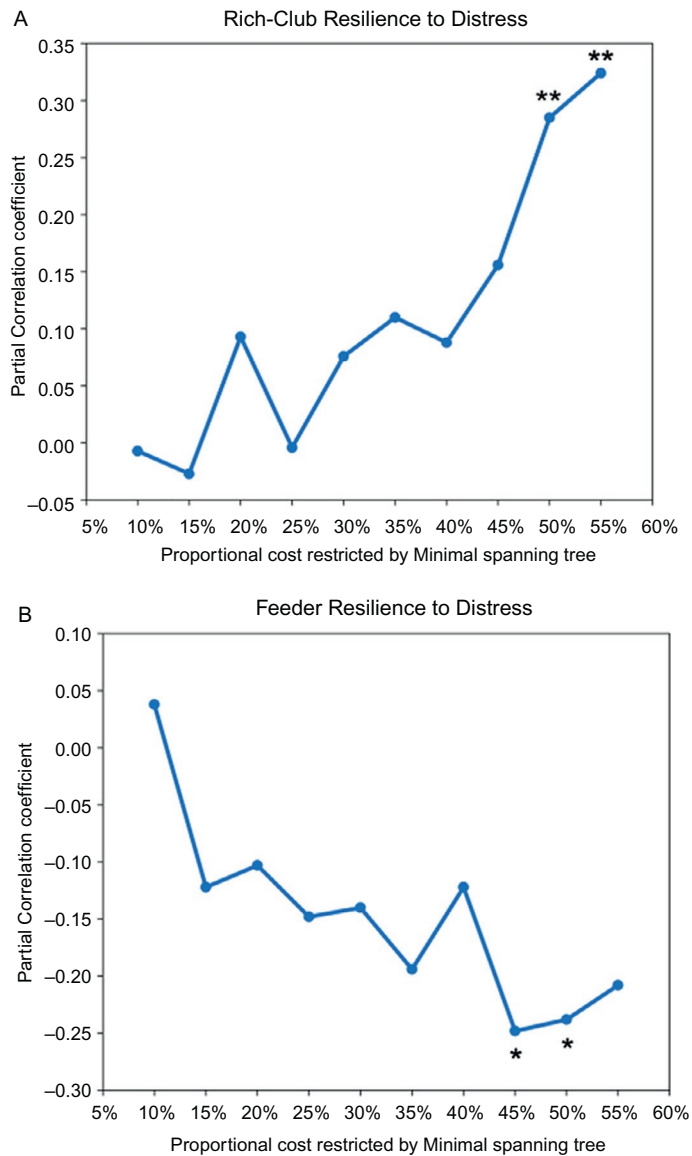
The relationship between the network efficiency and centrality of rich-club and feeder edges was evaluated using bivariate correlation. As in Fig. 5, rich-club centrality was significantly negatively correlated with network efficiency at network cost of 20% or higher. Similarly, feeder centrality was also significantly negatively correlated with network efficiency when the network cost was 30% or higher.

### **3.6 Network efficiency and resilience against removing selected edges**

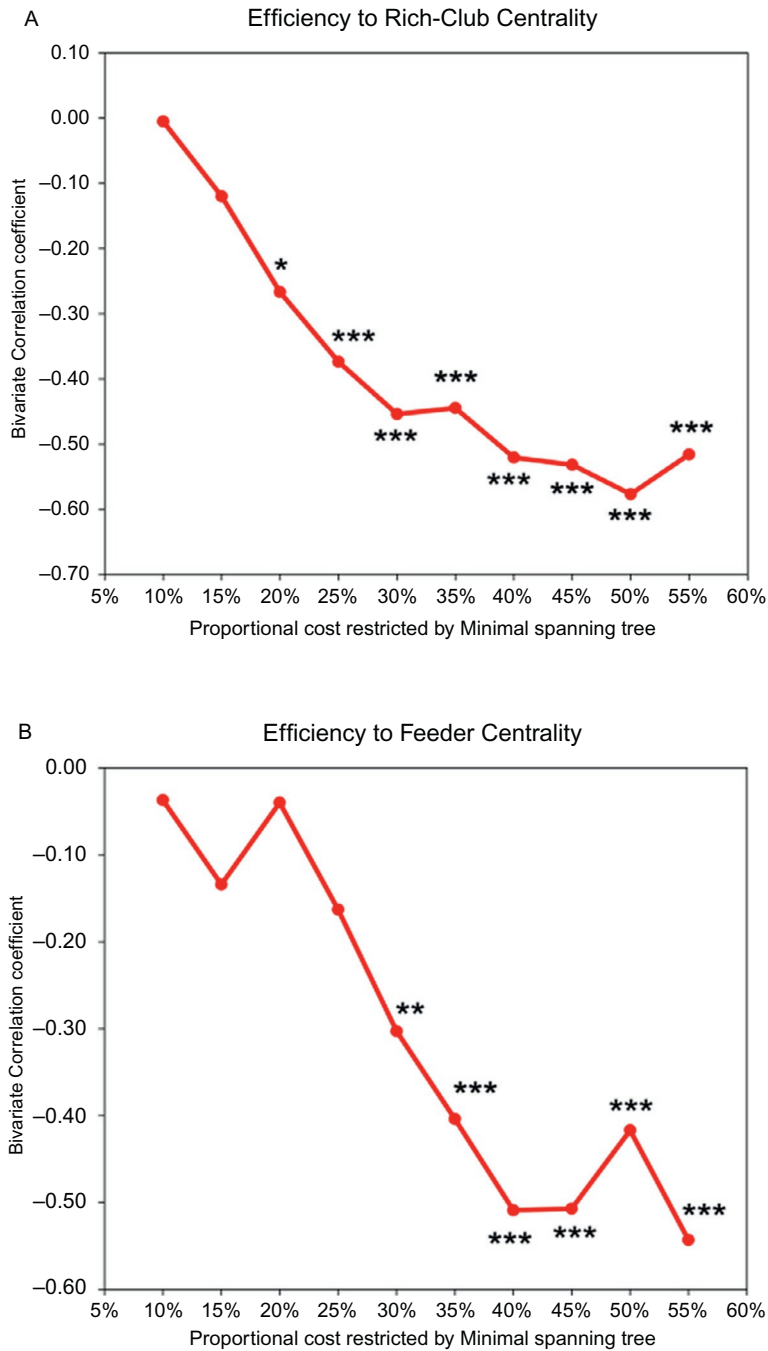
The trade-off between network efficiency and resilience measures was also quantified using bivariate correlation. As illustrated in Fig. 6, there was no significant relationship between the resilience against removing the rich-club edges and network

**FIG. 3**

Partial correlation of tinnitus-related distress to edge-betweenness centrality measures; (A) centrality of rich-club edges, and (B) centrality of feeder edges after controlling for age, mean hearing loss, loudness and duration. X-axis represents the proportional costs ranging from 10% to 55%, restricted using Minimal spanning tree algorithm. Y-axis is the partial correlation coefficient of distress to each measure (\* two-tailed  $P < 0.05$ , \*\*  $P < 0.01$ ).

**FIG. 4**

Partial correlation of tinnitus-related distress to network resilience measures; (A) resilience against removal of rich-club edges, and (B) resilience against removal of feeder edges after controlling for age, mean hearing loss, loudness and duration. X-axis represents the proportional costs ranging from 10% to 55%, restricted using Minimal spanning tree algorithm. Y-axis is the partial correlation coefficient of distress to each measure (\* two-tailed  $P < 0.05$ , \*\*  $P < 0.01$ ).

**FIG. 5**

Bivariate correlation of global network efficiency to centrality of important connections. (A) Efficiency and centrality of rich-club edges, and (B) efficiency and centrality of feeder edges (\* two-tailed  $P < 0.050$ , \*\*  $P < 0.010$ , \*\*\*  $P < 0.001$ ).

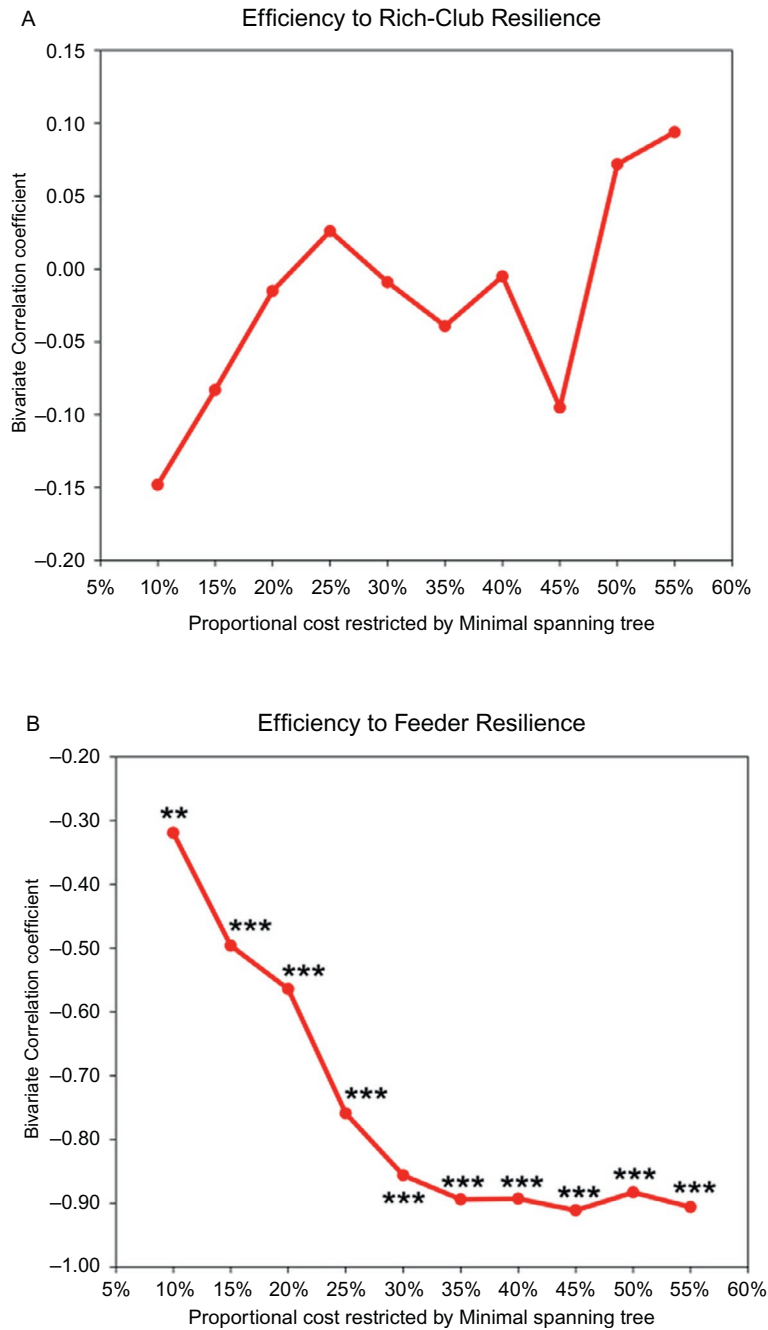


**FIG. 6**

Bivariate correlation of global network efficiency to network resilience against removing specific connections. Trade-off relationship is represented as the significant negative correlation between two. (A) Efficiency to resilience against removal of rich-club edges, and (B) efficiency to resilience against removal of feeder edges (\*\* two-tailed  $P < 0.010$ , \*\*\*  $P < 0.001$ ).

efficiency at any cost. On the other hand, the resilience for feeder edges showed significant negative correlation with the network efficiency at all costs. The magnitude of correlation appears to decrease as the cost decreases.

### 3.7 Path analysis on relationship between distress and network measures

Path analysis identified the relationship between the level of distress and efficiency of the network as influenced by other network parameters. The centrality of rich-club edges and resilience against removing feeder edges were found to be significantly correlated with both efficiency and distress at costs of 45% and 50%. Thus, path analysis was performed based on network measures computed at 45% and 50% costs. In the tested model, network efficiency and distress were either the primary predictor or the outcome, and rich-club centrality and feeder resilience were mediators between the predictor and the outcome. Fig. 7 visualizes all the path models tested in this study and signifies the model that best describes the relationship of variables, which is A-1. The comparative model indices of AIC and BIC at costs 45% and 50% are provided in Table 3.

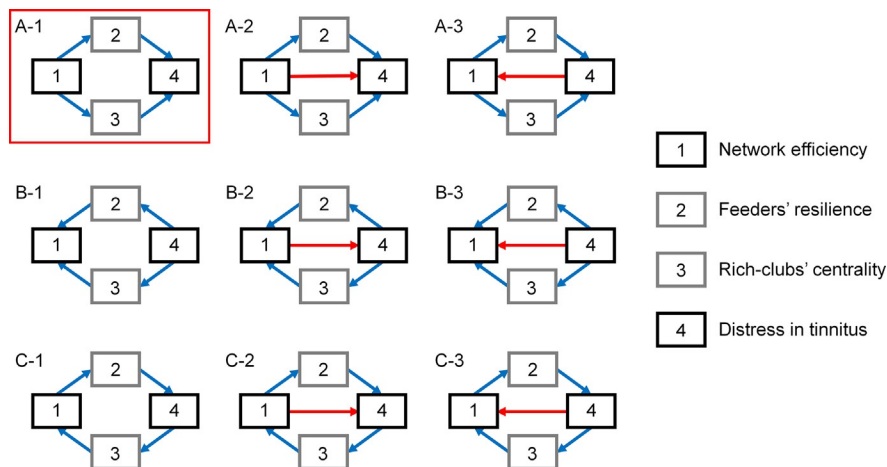


**FIG. 7**

Graphical representation for showing the paths based on the hypotheses. Alphabets (A, B, C) indicate the direction of the dependence between distress and network measures, and numbers (Honey et al., 2010; van den Heuvel et al., 2012; Xia et al., 2013) indicate the sub-models divided by whether the direct relationship between network efficiency and distress exists, and if it does, what the direction is. Red lines indicate that the regression coefficients between variables are positive, and blue lines indicate negative. According to the comparison of these indices in Table 3, Model A-1 is the best description of the relationship between variables, and is signified using a star mark next to the model name.

**Table 3** Goodness-of-fit indices for the models representing the relationship between the distress and network measures at the cost of 45% and 50%.

Model		GFI	AGFI	RMSEA	CFI	AIC	BIC
<i>Cost of 45%</i>							
A	A-1 *	0.999	0.997	0.000	1.000 *	16.118 *	36.116 *
	A-2	0.999	0.994	0.000	1.000	18.098	40.597
	A-3	0.999	0.994	0.000	1.000	18.098	40.596
B	B-1	0.917	0.587	0.297	0.917	33.680	53.678
	B-2	0.917	0.174	0.433	0.912	35.667	58.166
	B-3	0.917	0.174	0.433	0.912	35.660	58.158
C	C-1	0.999	0.994	0.000	1.000	16.203	36.201
	C-2	0.999	0.991	0.000	1.000	18.158	40.656
	C-3	0.999	0.991	0.000	1.000	18.158	40.656
<i>Cost of 50%</i>							
A	A-1 *	0.996	0.982	0.000	1.000 *	16.655 *	36.653 *
	A-2	0.997	0.970	0.000	1.000	18.542	41.040
	A-3	0.997	0.970	0.000	1.000	18.541	41.040
B	B-1	0.910	0.549	0.315	0.895	35.662	55.661
	B-2	0.910	0.100	0.457	0.890	37.597	60.095
	B-3	0.910	0.102	0.457	0.890	37.549	60.048
C	C-1	0.995	0.977	0.000	1.000	16.819	36.818
	C-2	0.997	0.965	0.000	1.000	18.622	41.120
	C-3	0.997	0.965	0.000	1.000	18.622	41.120

Note: Model A and sub-items represent the associations where network efficiency indirectly predicts distress. Model B and three sub-items represent the associations where distress indirectly predicts network efficiency. Model C and sub-items represent the loop where each variable predicts at least one other in the model, and none of the variables is solely independent. Comparison of CFI, AIC, BIC across models provides a possibly optimal model, which is model A-1 in cases of both costs of 45% and 50%. Abbreviations: GFI, goodness of fit index; AGFI, adjusted GFI; RMSEA, root mean square error of approximation; CFI, comparative fit index; AIC, Akaike information criterion; BIC, Bayesian information criterion. (\*indicates the relatively best model).

As shown in Table 3, indices for absolute goodness-of-fit showed that Models A-1, A-2, A-3, C-1, C-2 and C-3 adequately describe the relationship between variables. In comparison of relative indices among the models, AIC and BIC were the lowest for Model A-1 among the models tested, thus showing that Model A-1 explains the relationship of interest the best. Model A-1 represents that network efficiency predicts the level of distress in tinnitus, and that the feeders' resilience and rich-clubs' centrality are significantly mediating this relationship. Parameters were estimated using linear regression (Table 4), and the results show that there is a negative correlation of network efficiency to feeders' resilience and rich-clubs' centrality, and these two mediators correlate to distress in the negative direction. To note, the negative correlation of feeders' resilience and rich-clubs' centrality to distress was not significant within the model when they simultaneously predicted distress. These relations explain how an individual with higher network efficiency

**Table 4** Parameter estimations for the best model at costs 45% and 50% (Model A-1).

Independent variable →	Dependent variable	Beta	SE	P-value
<i>Cost of 45%</i>				
Global efficiency	Feeders' resilience	-0.910	0.044	<0.001
Global efficiency	Rich-Clubs' centrality	-0.522	0.090	<0.001
Feeders' resilience	Distress	-0.151	0.115	0.188
Rich-Clubs' centrality	Distress	-0.209	0.115	0.068
Error	Global efficiency	0.944	0.142	<0.001
Error	Feeders' resilience	0.162	0.024	<0.001
Error	Rich-Clubs' centrality	0.687	0.103	<0.001
Error	Distress	0.854	0.128	<0.001
<i>Cost of 50%</i>				
Global efficiency	Feeders' resilience	-0.877	0.051	<0.001
Global efficiency	Rich-Clubs' centrality	-0.578	0.087	< 0.001
Feeders' resilience	Distress	-0.157	0.118	0.183
Rich-Clubs' centrality	Distress	-0.170	0.118	0.150
Error	Global efficiency	0.944	0.142	<0.001
Error	Feeders' resilience	0.218	0.033	<0.001
Error	Rich-Clubs' centrality	0.629	0.094	<0.001
Error	Distress	0.870	0.130	<0.001

Note: Parameter estimates are shown as beta (standardized regression coefficient) and standard error (SE) values, and the significance of the parameter estimation is shown as P-values. Independent predicts the dependent variables as shown in Model A-1. Error variables correspond to each of the endogenous variables.

may develop a higher level of tinnitus-related distress. Current results on path analysis are consistent for both costs of 45% and 50%, as in [Tables 3 and 4](#).

## 4 Discussion

This study assessed the predictive relationship between tinnitus distress and the global efficiency of the functional network of tinnitus patients mediated by its resilience and edge-betweenness centrality using rsfMRI. This was performed by separately computing the resilience and centrality of the rich-club and feeder connections and analyzing their relationship with tinnitus distress and global efficiency of the network using path analysis.

### 4.1 Distress-efficiency and its relation to functional integration and segregation

The results show a positive correlation between tinnitus distress and efficiency of information transfer between regions. This is a robust finding across different network costs showing that this is not an effect of spurious connections in the network.

Furthermore, the proportional thresholding method such as the one applied in this study has also been shown to produce stable network metrics compared to absolute network thresholding (Garrison et al., 2015; van den Heuvel et al., 2017). In addition, it also ensures that the topological effects produced are reliably separated from the density of the network (Ginestet et al., 2011; van den Heuvel et al., 2017). Higher global efficiency of a pathological network has been noted with other disorders such as major depression, schizophrenia, and post-traumatic stress disorder (Lei et al., 2015; Lo et al., 2015; Zhang et al., 2011). Furthermore, our results also show significant and robust negative relationship of path length and positive relationship of clustering coefficient and small-worldness of the network with distress across a range of costs. These results are in accordance with the findings of our previous study using resting state EEG, where we showed a significant negative relationship of characteristic path length and a positive relationship of clustering coefficient of networks with distress in patients with high distress compared to patients with low distress (Mohan et al., 2018). The higher small-worldness parameter in patients with high distress in the current study suggests that the network may be reconfiguring to a more random topology (Humphries and Gurney, 2008). Given the robust finding across a range of proportionally thresholded costs, we can say with confidence that is not a result of spurious connections (Garrison et al., 2015; Ginestet et al., 2011; van den Heuvel et al., 2017).

## 4.2 Distress-efficiency and its relation to centrality and resilience of rich-club and feeder nodes

To better understand how global efficiency of the network affects distress through changes in network topology, we investigated the relationship between distress, resilience and centrality of the rich-club and feeder connections and the efficiency of the network. On the one hand, the efficiency of the network was significantly negatively correlated with the resilience of the feeder network, and not with that of the rich-club network. Furthermore, the resilience of the feeder network was negatively correlated with distress. On the other hand, although the efficiency of the network was negatively correlated with the mean edge-betweenness centrality of both the rich-club and feeder connections only the mean edge-betweenness centrality of the rich-club connections was negatively correlated with distress. Thus, performing a path analysis using the above variables, we observed that changes in network efficiency of the tinnitus network positively affected changes in distress and was significantly mediated by the resilience of the feeder network and mean edge-betweenness centrality of the rich-club network.

We observe that this relationship holds only at very high costs i.e. at 45% and 50%. Previous studies showed that real networks between the range of 37% and 50% showed small-world characteristics and lower sensitivity to individual variability (Lynall et al., 2010), and that networks above 50% contained spurious connections were non-biological making network properties unreliable (Humphries et al., 2006; Kaiser and Hilgetag, 2006). In the current study, we observe that the

path analysis models for a significant relationship between distress and network efficiency hold for network costs in the range of biological acceptance. This suggests that this relationship is a physiological occurrence in tinnitus patients and not a result of spurious network connectivity.

### 4.3 Predictive Relationship between Tinnitus Distress and Network Efficiency

From the results of the above model, we observe that the efficiency–resilience and efficiency–centrality trade-offs play an important role in mediating tinnitus-related distress. The resilience–efficiency imbalance shows that higher the efficiency of information transfer, lower the resilience of the feeders. Such an imbalance suggests a reorganization towards a less resilient and more efficient topology (Netotea and Pongor, 2006). Furthermore, based on the results of our previous study, we understand that there exists an underlying difference in the resilience of the rich-club and the feeder network to external attacks (Mohan et al., 2017). The rich-club network was shown to be more resilient to a virtual lesion than the feeder network. Furthermore, Crossley and colleagues suggest that disorders affect the regions that are less resilient or more vulnerable to external attacks (Crossley et al., 2014). This fits with the results of the current study showing that lower resilience of the feeder network is directly related to higher tinnitus-related distress.

From the efficiency–centrality trade-off we observe that the higher the efficiency of the network, the lower the centrality of the rich-club network. The main role of the rich-club is to integrate the hubs of the network promoting small-worldness characteristics (Bullmore and Sporns, 2012). However, the higher clustering coefficient and small-worldness and lower path length of the network in patients with higher distress suggests a more random topology. This supports the idea that the rich-club becomes less important in binding the hubs of the network. Thus, higher network efficiency and lower centrality of the rich-club suggests that the network is reconfiguring towards a more random topology in patients with higher distress.

### 4.4 Effects of the tinnitus stressor on brain networks

The higher values of distress, influenced by a positive change in network efficiency, may be considered as a stress response to a chronic stressor, i.e. tinnitus. This could be explained by Lazarus and Folkman’s Cognitive Transactional Theory of Stress (Biggs et al., 2017; Lazarus, 1986). They proposed that the stress response depends on the ability of the individual to cope with stress caused by the stressor. An important component of this theory was the notion of appraisal, which is defined as the process of categorizing the effect of the stress with respect to personal well-being (Lazarus, 1986). This appraisal plays a critical role in mediating the response to stress. Thus, in this process of evaluative appraisal, if the stress is considered positive or challenging (i.e. learning a new task), then there may not be a stress response. On the other hand, if stress is considered negative or threatening, this then leads to a

stress response. In the context of the brain, tinnitus may be considered the stressor. In the current study, the positive change in tinnitus network efficiency negatively influences the resilience of the feeder network and the betweenness centrality of the rich-club network which mediates a positive change in tinnitus-related distress. Applying the concept of the Cognitive Transactional Theory of Stress, we propose that in patients with higher network efficiency, the brain possibly perceives the lower resilience of the feeders and centrality of the rich-club as a threat to the system's topological equilibrium reflecting in higher distress in these patients. Such a maladaptive network reorganization, which is paradoxically more efficient, may be a possible explanation as to why tinnitus patients are stuck thinking about their percept all the time.

#### 4.5 Future Directions

The current study is the first study, that we know of, to establish a relationship between tinnitus distress and the global efficiency of a network as mediated by other network parameters. The present results show that as the network becomes more efficient, the tinnitus-related distress becomes higher. This could mean that the networks of patients with high distress are paradoxically more efficient in transferring information about tinnitus and may be the reason why these patients are so focused on their percept compared to anything else they do. It would also be worthwhile for future studies to confirm the results of the current study using an appropriate control group with no tinnitus. Furthermore, since fMRI lacks good temporal resolution, it would also be worthwhile to replicate this study using resting state EEG or MEG to understand the role of different frequency bands in the mediation of the relationship between tinnitus distress and efficiency of the network. The current study could thus provide a general explanation as to what happens to a chronically distressed brain. Since distress is a domain-general symptom, that not only accompanies tinnitus but other disorders, the results of the current study may present the neural correlates of chronic distress in general.

---

### 5 Conclusion

This study describes, in detail, the relationship between tinnitus-related distress and various network properties. It further establishes an association between distress, resilience and centrality of the feeders and rich-club connections, and the efficiency of the network. We observe that the resilience of the feeder connections and centrality of the rich-club connections significantly mediate the relationship between distress and network efficiency in such a way that, the higher the network efficiency, the lower the resilience of the feeders and centrality of the rich-club, in turn reflects in higher distress in tinnitus patients. This relationship may be explained as a stress response of the brain to the tinnitus stressor, where the higher efficiency of the network is associated with a decrease in the resilience of the feeders and centrality of the rich-club connections.

---

## Ethical statement

This study was approved by the local ethical committee (Antwerp University Hospital) and was in accordance with the Declaration of Helsinki. Collection of the data was under approval of IRB UZA OGA85. All patients gave a written informed consent.

---

## Disclosure

The authors report no conflicts of interest.

---

## Author contributions

HBY: Data analysis, preparing manuscript.

AM: Preparing manuscript.

DDR: Data collection, data analysis.

SV: Data collection, data analysis.

---

## Data accessibility statement

The data is present with the corresponding author and may be available on request.

---

## References

- Achard, S., Bullmore, E., 2007. Efficiency and cost of economical brain functional networks. *PLoS Comput. Biol.* 3, e17.
- Aldrich, E., 2010. Wavelets: A package of functions for computing wavelet filters, wavelet transforms and multiresolution analyses. R package version 0.2-6.
- Alstott, J., Breakspear, M., Hagmann, P., Cammoun, L., Sporns, O., 2009. Modeling the impact of lesions in the human brain. *PLoS Comput. Biol.* 5, e1000408.
- Arbuckle, J., 2013. IBM SPSS AMOS 22 Users' Guide. IBM Corp.
- Ashburner, J., Friston, K.J., 1999. Nonlinear spatial normalization using basis functions. *Hum. Brain Mapp.* 7, 254–266.
- Audiology, B.S.o. (2008) Recommended procedure: pure tone air and bone conduction threshold audiometry with and without masking and determination of uncomfortable loudness levels.
- Behzadi, Y., Restom, K., Liau, J., Liu, T.T., 2007. A component based noise correction method (CompCor) for BOLD and perfusion based fMRI. *Neuroimage* 37, 90–101.
- Biggs, A., Brough, P., Drummond, S., 2017. Lazarus and Folkman's psychological stress and coping theory. In: *The Handbook of Stress and Health: A Guide to Research and Practice*, pp. 349–364.
- Biswal, B., Zerrin Yetkin, F., Haughton, V.M., Hyde, J.S., 1995. Functional connectivity in the motor cortex of resting human brain using echo-planar mri. *Magn. Reson. Med.* 34, 537–541.

- Boccaletti, S., Latora, V., Moreno, Y., Chavez, M., Hwang, D.U., 2006. Complex networks: structure and dynamics. *Phys. Rep.* 424, 175–308.
- Brede, M., de Vries, B.J., 2009. Networks that optimize a trade-off between efficiency and dynamical resilience. *Phys. Lett. A* 373, 3910–3914.
- Bullmore, E., Sporns, O., 2012. The economy of brain network organization. *Nat. Rev. Neurosci.* 13, 336–349.
- Chen, Y.C., Xia, W., Chen, H., Feng, Y., Xu, J.J., Gu, J.P., Salvi, R., Yin, X., 2017. Tinnitus distress is linked to enhanced resting-state functional connectivity from the limbic system to the auditory cortex. *Hum. Brain Mapp.*
- Colizza, V., Flammini, A., Serrano, M.A., Vespignani, A., 2006. Detecting rich-club ordering in complex networks. *Nat. Phys.* 2, 110–115.
- Collin, G., Sporns, O., Mandl, R.C., van den Heuvel, M.P., 2014. Structural and functional aspects relating to cost and benefit of rich club organization in the human cerebral cortex. *Cereb. Cortex* 24, 2258–2267.
- Crossley, N.A., Mechelli, A., Scott, J., Carletti, F., Fox, P.T., McGuire, P., Bullmore, E.T., 2014. The hubs of the human connectome are generally implicated in the anatomy of brain disorders. *Brain* 137, 2382–2395.
- Cuzzocrea, A., Papadimitriou, A., Katsaros, D., Manolopoulos, Y., 2012. Edge betweenness centrality: a novel algorithm for QoS-based topology control over wireless sensor networks. *J. Netw. Comput. Appl.* 35, 1210–1217.
- De Ridder, D., Vanneste, S., Congedo, M., 2011. The distressed brain: a group blind source separation analysis on tinnitus. *PLoS One* 6, e24273.
- De Ridder, D., Vanneste, S., Weisz, N., Londero, A., Schlee, W., Elgoyhen, A.B., Langguth, B., 2014. An integrative model of auditory phantom perception: tinnitus as a unified percept of interacting separable subnetworks. *Neurosci. Biobehav. Rev.* 44, 16–32.
- Desikan, R.S., Ségonne, F., Fischl, B., Quinn, B.T., Dickerson, B.C., Blacker, D., Buckner, R.L., Dale, A.M., Maguire, R.P., Hyman, B.T., 2006. An automated labeling system for subdividing the human cerebral cortex on MRI scans into gyral based regions of interest. *Neuroimage* 31, 968–980.
- D’Esposito, M., Deouell, L.Y., Gazzaley, A., 2003. Alterations in the BOLD fMRI signal with ageing and disease: a challenge for neuroimaging. *Nat. Rev. Neurosci.* 4, 863–872.
- Eggermont, J.J., Roberts, L.E., 2004. The neuroscience of tinnitus. *Trends Neurosci.* 27, 676–682.
- Frazier, J.A., Chiu, S., Breeze, J.L., Makris, N., Lange, N., Kennedy, D.N., Herbert, M.R., Bent, E.K., Koneru, V.K., Dieterich, M.E., 2005. Structural brain magnetic resonance imaging of limbic and thalamic volumes in pediatric bipolar disorder. *Am. J. Psychiatry* 162, 1256–1265.
- Friston, K., 2010. The free-energy principle: a unified brain theory? *Nat. Rev. Neurosci.* 11, 127–138.
- Friston, K., Ashburner, J., Frith, C.D., Poline, J.B., Heather, J.D., Frackowiak, R.S., 1995. Spatial registration and normalization of images. *Hum. Brain Mapp.* 3, 165–189.
- Garrison, K.A., Scheinost, D., Finn, E.S., Shen, X., Constable, R.T., 2015. The (in)stability of functional brain network measures across thresholds. *Neuroimage* 118, 651–661.
- Ginestet, C.E., Nichols, T.E., Bullmore, E.T., Simmons, A., 2011. Brain network analysis: separating cost from topology using cost-integration. *PLoS ONE* 6, e21570.
- Girvan, M., Newman, M.E., 2002. Community structure in social and biological networks. *Proc. Natl. Acad. Sci.* 99, 7821–7826.

- Glerean, E., Salmi, J., Lahnakoski, J.M., Jääskeläinen, I.P., Sams, M., 2012. Functional magnetic resonance imaging phase synchronization as a measure of dynamic functional connectivity. *Brain Connect.* 2, 91–101.
- Hagmann, P., Cammoun, L., Gigandet, X., Meuli, R., Honey, C.J., Wedeen, V.J., Sporns, O., 2008. Mapping the structural core of human cerebral cortex. *PLoS Biol.* 6, e159.
- Hallam, R., 1996. *Manual of the Tinnitus Questionnaire (TQ)*. Psychological Corporation, London.
- Heller, A.J., 2003. Classification and epidemiology of tinnitus. *Otolaryngol. Clin. North Am.* 36, 239–248.
- Hidalgo, C.A., Klinger, B., Barabási, A.-L., Hausmann, R., 2007. The product space conditions the development of nations. *Science* 317, 482–487.
- Hiller, W., Goebel, G., 1992. A psychometric study of complaints in chronic tinnitus. *J. Psychosom. Res.* 36, 337–348.
- Hiller, W., Goebel, G., Rief, W., 1994. Reliability of self-rated tinnitus distress and association with psychological symptom patterns. *Br. J. Clin. Psychol.* 33 (Pt 2), 231–239.
- Holling, C.S., 1973. Resilience and stability of ecological systems. *Annu. Rev. Ecol. Syst.* 4, 1–23.
- Holme, P., 2005. Core-periphery organization of complex networks. *Phys. Rev. E* 72, 046111.
- Honey, C.J., Thivierge, J.P., Sporns, O., 2010. Can structure predict function in the human brain? *Neuroimage* 52 (3), 766–776.
- Hsu, L., Self, S.G., Grove, D., Randolph, T., Wang, K., Delrow, J.J., Loo, L., Porter, P., 2005. Denoising array-based comparative genomic hybridization data using wavelets. *Biostatistics* 6, 211–226.
- Humphries, M.D., Gurney, K., 2008. Network ‘small-world-ness’: a quantitative method for determining canonical network equivalence. *PLoS One* 3, e0002051.
- Humphries, M.D., Gurney, K., Prescott, T.J., 2006. The brainstem reticular formation is a small-world, not scale-free, network. *Proc. Biol. Sci.* 273, 503–511.
- Imperatori, C., Farina, B., Quintiliani, M.I., Onofri, A., Gattinara, P.C., Lepore, M., Gnoni, V., Mazzucchi, E., Contardi, A., Della Marca, G., 2014. Aberrant EEG functional connectivity and EEG power spectra in resting state post-traumatic stress disorder: a sLORETA study. *Biol. Psychol.* 102, 10–17.
- Kaiser, M., Hilgetag, C.C., 2006. Nonoptimal component placement, but short processing paths, due to long-distance projections in neural systems. *PLoS Comput. Biol.* 2, e95.
- Kross, E., Egner, T., Ochsner, K., Hirsch, J., Downey, G., 2007. Neural dynamics of rejection sensitivity. *J. Cogn. Neurosci.* 19, 945–956.
- Landgrebe, M., Barta, W., Rosengarth, K., Frick, U., Hauser, S., Langguth, B., Rutschmann, R., Greenlee, M.W., Hajak, G., Eichhammer, P., 2008. Neuronal correlates of symptom formation in functional somatic syndromes: a fMRI study. *Neuroimage* 41, 1336–1344.
- Latora, V., Marchiori, M., 2001. Efficient behavior of small-world networks. *Phys. Rev. Lett.* 87, , 198701.
- Latora, V., Marchiori, M., 2003. Economic small-world behavior in weighted networks. *Eur. Phys. J. B* 32, 249–263.
- Lazarus, R.S., 1986. Folkman, S. (1984). *Stress, Appraisal, and Coping*. Springer, New York.
- Lei, D., Li, K., Li, L., Chen, F., Huang, X., Lui, S., Li, J., Bi, F., Gong, Q., 2015. Disrupted functional brain connectome in patients with posttraumatic stress disorder. *Radiology* 276, 818–827.

- Lo, C.-Y.Z., Su, T.-W., Huang, C.-C., Hung, C.-C., Chen, W.-L., Lan, T.-H., Lin, C.-P., Bullmore, E.T., 2015. Randomization and resilience of brain functional networks as systems-level endophenotypes of schizophrenia. *Proc. Natl. Acad. Sci.* 112, 9123–9128.
- Lynall, M.-E., Bassett, D.S., Kerwin, R., McKenna, P.J., Kitzbichler, M., Muller, U., Bullmore, E., 2010. Functional connectivity and brain networks in schizophrenia. *J. Neurosci.* 30, 9477–9487.
- Makris, N., Goldstein, J.M., Kennedy, D., Hodge, S.M., Caviness, V.S., Faraone, S.V., Tsuang, M.T., Seidman, L.J., 2006. Decreased volume of left and total anterior insular lobule in schizophrenia. *Schizophr. Res.* 83, 155–171.
- McAuley, J.J., da Fontoura Costa, L., Caetano, T.S., 2007. Rich-club phenomenon across complex network hierarchies. *Appl. Phys. Lett.* 91, 084103.
- McCombe, A., Baguley, D., Coles, R., McKenna, L., McKinney, C., Windle-Taylor, P., 2001. Guidelines for the grading of tinnitus severity: the results of a working group commissioned by the British Association of Otolaryngologists, head and neck surgeons, 1999. *Clin. Otolaryngol. Allied Sci.* 26, 388–393.
- Meeus, O., Blaivie, C., Van de Heyning, P., 2007. Validation of the Dutch and the French version of the tinnitus questionnaire. *B-ENT 3 (Suppl 7)*, 11–17.
- Meeus, O., Heyndrickx, K., Lambrechts, P., De Ridder, D., Van de Heyning, P., 2009. Phase-shift treatment for tinnitus of cochlear origin. *Eur. Arch. Otorhinolaryngol.* 267, 881–888.
- Meeus, O., De Ridder, D., Van de Heyning, P., 2011. Administration of the combination clonazepam-deanxit as treatment for tinnitus. *Otol. Neurotol.* 32, 701–709.
- Mohan, A., De Ridder, D., Vanneste, S., 2016a. Emerging hubs in phantom perception connectomics. *NeuroImage Clin.* 11, 181–194.
- Mohan, A., De Ridder, D., Vanneste, S., 2016b. Graph theoretical analysis of brain connectivity in phantom sound perception. *Sci. Rep.* 6, 19683.
- Mohan, A., De Ridder, D., Vanneste, S., 2017. Robustness and dynamicity of functional networks in phantom sound. *Neuroimage* 146, 171–187.
- Mohan, A., Alexandra, S.J., Johnson, C.V., De Ridder, D., Vanneste, S., 2018. Effect of distress on transient network dynamics and topological equilibrium in phantom sound perception. *Prog. Neuropsychopharmacol. Biol. Psychiatry* 84, 79–92.
- Moisset, X., Bouhassira, D., 2007. Brain imaging of neuropathic pain. *Neuroimage* 37, S80–S88.
- Netotea, S., Pongor, S., 2006. Evolution of robust and efficient system topologies. *Cell. Immunol.* 244, 80–83.
- Peng, G.-S., Tan, S.-Y., Wu, J., Holme, P., 2016. Trade-offs between robustness and small-world effect in complex networks. *Sci. Rep.* 6, 37317.
- Percival, D.B., Walden, A.T., 2000. *Wavelet Methods for Time Series Analysis*. Cambridge Series in Statistical and Probabilistic Mathematics.
- Ponce-Alvarez, A., Deco, G., Hagmann, P., Romani, G.L., Mantini, D., Corbetta, M., 2015. Resting-state temporal synchronization networks emerge from connectivity topology and heterogeneity. *PLoS Comput. Biol.* 11, e1004100.
- Rubinov, M., Sporns, O., 2010. Complex network measures of brain connectivity: uses and interpretations. *Neuroimage* 52, 1059–1069.
- Schank, T., Wagner, D., 2004. *Approximating Clustering-Coefficient and Transitivity*. Universität Karlsruhe, Fakultät für Informatik.
- Schreiber, J.B., Nora, A., Stage, F.K., Barlow, E.A., King, J., 2006. Reporting structural equation modeling and confirmatory factor analysis results: a review. *J. Educ. Res.* 99, 323–338.

- Schumacker, R.E., Lomax, R.G., 2012. *A Beginner's Guide to Structural Equation Modeling*. Routledge.
- Senden, M., Deco, G., de Reus, M.A., Goebel, R., van den Heuvel, M.P., 2014. Rich club organization supports a diverse set of functional network configurations. *Neuroimage* 96, 174–182.
- Song, J.-J., Vanneste, S., Schlee, W., Van de Heyning, P., De Ridder, D., 2015. Onset-related differences in neural substrates of tinnitus-related distress: the anterior cingulate cortex in late-onset tinnitus, and the frontal cortex in early-onset tinnitus. *Brain Struct. Funct.* 220, 571–584.
- Stam, C.J., 2014. Modern network science of neurological disorders. *Nat. Rev. Neurosci.* 15, 683–695.
- Team, R.C., 2013. R: A Language and Environment for Statistical Computing.
- van den Heuvel, M.P., Sporns, O., 2011. Rich-club organization of the human connectome. *J. Neurosci.* 31, 15775–15786.
- van den Heuvel, M.P., Kahn, R.S., Goñi, J., Sporns, O., 2012. High-cost, high-capacity backbone for global brain communication. *Proc. Natl. Acad. Sci. U.S.A.* 109 (28), 11372–11377.
- van den Heuvel, M.P., de Lange, S.C., Zalesky, A., Seguin, C., Yeo, B.T., Schmidt, R., 2017. Proportional thresholding in resting-state fMRI functional connectivity networks and consequences for patient-control connectome studies: issues and recommendations. *Neuroimage* 152, 437–449.
- Vanneste, S., Congedo, M., De Ridder, D., 2014. Pinpointing a highly specific pathological functional connection that turns phantom sound into distress. *Cereb. Cortex* 24, 2268–2282.
- von Leupoldt, A., Sommer, T., Kegat, S., Baumann, H.J., Klose, H., Dahme, B., Büchel, C., 2009. Dyspnea and pain share emotion-related brain network. *Neuroimage* 48, 200–206.
- Wager, T.D., Atlas, L.Y., Lindquist, M.A., Roy, M., Woo, C.-W., Kross, E., 2013. An fMRI-based neurologic signature of physical pain. *N. Engl. J. Med.* 368, 1388–1397.
- Watts, D.J., Strogatz, S.H., 1998. Collective dynamics of 'small-world' networks. *Nature* 393, 440–442.
- Whitfield-Gabrieli, S., Nieto-Castanon, A., 2012. Conn: a functional connectivity toolbox for correlated and anticorrelated brain networks. *Brain Connect.* 2, 125–141.
- Xia, H., Asif, I., Zhao, X., 2013. Cloud-ECG for real time ECG monitoring and analysis. *Comput. Methods Programs Biomed.* 110 (3), 253–259.
- Yang, J., Leskovec, J., 2014. *Overlapping Communities Explain Core-Periphery Organization of Networks*. Stanford University.
- Zalesky, A., Fornito, A., Cocchi, L., Gollo, L.L., van den Heuvel, M.P., Breakspear, M., 2016. Connectome sensitivity or specificity: which is more important? *Neuroimage* 142, 407–420.
- Zhang, J., Wang, J., Wu, Q., Kuang, W., Huang, X., He, Y., Gong, Q., 2011. Disrupted brain connectivity networks in drug-naive, first-episode major depressive disorder. *Biol. Psychiatry* 70, 334–342.